Variational Integrators for the Gravitational N-Body Problem

Will M. Farr

and

Edmund Bertschinger

Department of Physics and Kavli Institute for Astrophysics and Space Research, MIT
Room 37-602A, 77 Massachusetts Ave., Cambridge, MA 02139

farr@mit.edu, edbert@mit.edu

ABSTRACT

This paper describes a novel fourth-order integration algorithm for the gravitational N-body problem based on discrete Lagrangian mechanics. When used with shared timesteps, the algorithm is momentum conserving and symplectic. We generalize the algorithm to handle individual time steps; this introduces fifth-order errors in angular momentum conservation and symplecticity. We show that using block power of two timesteps does not increase the error in symplecticity. In contrast to other high-order, symplectic, momentum-preserving algorithms in widespread astrophysical use, the algorithm takes only forward timesteps. We compare a code integrating an N-body system using the algorithm with a direct-summation force calculation to standard stellar cluster simulation codes. We find that our algorithm has significantly better symplecticity and momentum conservation errors than standard algorithms for equivalent numbers of potential evaluations and equivalent energy conservation errors.

Subject headings: methods: N-body simulations — methods: numerical

1. Introduction

The gravitational N-body problem is the numerical integration of trajectories for N particles with pairwise inverse square-law forces. Ideally, a numerical method should respect all of the symmetries of the exact problem. Conservation of linear and angular momentum and energy — in toto or in pairwise interactions — are often used as quality indicators for numerical algorithms. However, there is another conservation law following from Hamiltonian dynamics: conservation of phase space volume.

Hamiltonian systems describe incompressible flow in phase space (q, p) where q is a vector of generalized coordinates and p is the vector of corresponding canonical momenta. Compressible flow, in contrast with Hamiltonian flow, is dissipative. Dissipation leads to unphysical heat transport in N-body systems, even if energy is conserved exactly. Because self-gravitating systems have negative specific heats, dissipative evolution can lead to instability.

Symplectic integration methods avoid unphysical dissipation by conserving exactly the phase space volume. Symplectic methods are well known in numerical integration of the solar system following the pioneering work of Wisdom & Holman (1991). However, the advantages of symplectic methods apply to systems with many more bodies. Indeed, cosmological simulations with millions or even billions of particles often use the leapfrog method because of its symplectic behavior (Springel 2005b; Shirokov & Bertschinger 2005).

The leapfrog algorithm is second-order accurate. Higher-order accurate algorithms are possible but conventionally require substeps integrated backwards in time (Yoshida 1993; Chambers 2003) and such techniques typically require many more potential evaluations than standard integrators. Below we present a fourth-order symplectic algorithm with only two potential evaluations per step that requires solution of a nonlinear algebraic equation for one forwards substep. If the nonlinear equation is solved approximately by iteration then the algorithm is approximately symplectic with an error in phase space conservation that can be made arbitrarily small. In contrast to other astrophysically well-known symplectic algorithms, our algorithm is derived from a discrete variational principle.

Gravitating systems typically have a large dynamic range of density and hence dynamical time, making it computationally inefficient to use a constant timestep, as required by most symplectic algorithms. Either adaptive timesteps (which change with time as a system evolves), individual timesteps (which differ for each particle), or both are required to make a computation feasible. This is especially true when unsoftened inverse-square law forces are used, e.g., in numerical simulation of globular clusters (Heggie & Hut 2003).

It is widely believed that adaptive timesteps are incompatible with symplecticity but we show otherwise in Section 3. This assumed breakdown of symplecticity, coupled with the large number of potential evaluations for standard higher-order symplectic methods, has led researchers to seek alternative ways to reduce dissipation, e.g. using time-reversible integration (Preto & Tremaine 1999; Makino et al. 1996). These techniques treat the symptoms of non-symplecticity (linear growth in various errors) without treating the cause (non-conservation of the symplectic form). Our algorithm addresses the cause, and we see corresponding improvements in symplecticity and momentum conservation for equivalent energy error to relative standard algorithms.

In this paper we present a new fourth-order integrator requiring only two force evaluations per timestep, which is fifth-order in its phase space conservation (symplecticity). Each additional force evaluation improves the symplecticity by two powers of the timestep. We analyze the breakdown of symplecticity when adaptive and individual timesteps are used and show that symplecticity is effectively restored when block power of two timesteps are used.

The algorithm is based on a discrete approximation to the action of a system, described in Section 2. Adaptive, individual, and combined block timesteps are discussed in Sections 3, 4, and 5 respectively. Numerical tests are presented in Section 6. Conclusions are given in Section 7.

2. Variational Integrators

Variational integrators are based on applying Hamilton's principle of stationary action to discrete approximations to the action for a physical system. Lew et al. (2004) is an excellent introduction to variational integrators in an engineering context; Marsden & West (2001) provides a much more mathematical discussion, including proofs of the essential properties of variational integrators and many examples of particular integration rules. This section is a brief introduction to variational integrators. Here and throughout we suppress vector indices on variables (juxtaposition of variables thus denotes multiplication in the one-dimensional case and the usual dot-product in the multidimensional case). We denote the derivative of the function f by Df; we denote the partial derivative on the ith argument of the function g by $\partial_i g$ (argument labels begin at 0).

The fundamental theorem of variational integration (Marsden & West 2001, Theorem 2.3.1) states that if H is an approximation to the action of a mechanical system,

$$H(h, q_1, q', q'', \ldots, q^{(n)}, q_2) = S[q](t_1, t_1 + h) + \mathcal{O}(h^{r+1}) = \int_{t_1}^{t_1+h} dt\, L(t, q(t), Dq(t)) + \mathcal{O}(h^{r+1}), \tag{1}$$

where $q_1 = q(t_1)$, $q_2 = q(t_2)$, the $q^{(i)}$ are intermediate positions in the time interval $[t_1, t_1 + h]$, S is the action functional and L is the Lagrangian for the system, then the equations

$$\partial_1 H(h, q_1, q', q'', \ldots, q^{(n)}, q_2) = -p_1 \tag{2a}$$

$$\partial_i H(h, q_1, q', q'', \ldots, q^{(n)}, q_2) = 0, \qquad i = 2, 3, \ldots, n+1 \tag{2b}$$

$$\partial_{n+2} H(h, q_1, q', q'', \ldots, q^{(n)}, q_2) = p_2 \tag{2c}$$

define a map $(q_1, p_1) \mapsto (q_2, p_2)$ which is an order r integrator for the mechanical system. The function H is called the *discrete Lagrangian*. Equations (2b) extremize the discrete

action approximation with respect to the discrete path $\{q^{(i)}\}$, while equations (2a) and (2c) exploit that the action is a F_1-type generating function for the time-evolution canonical transformation (Sussman et al. 2001, pp. 415–416).

The map defined by equations (2) has many useful properties analogous to the properties of the exact evolution of the system defined by L. First, it is momentum-preserving: imagine an infinitesimal variation in the coordinates q_1, q_2 and $q^{(i)}$ which leaves H invariant when q_1, the $q^{(i)}$ and q_2 satisfy equations (2). We have

$$\delta H = \partial_1 H(h, q_1, q', q'', \ldots, q^{(n)}, q_2)\delta q_1 + \sum_{i=2}^{n+1} \partial_i H(h, q_1, q', q'', \ldots, q^{(n)}, q_2)\delta q^{(i)} + \partial_{n+2} H(h, q_1, q', q'', \ldots, q^{(n)}, q_2)\delta q_2 = p_2 \delta q_2 - p_1 \delta q_1 = 0. \quad (3)$$

In this situation the quantity $p\delta q$ is conserved by the integrator: this is the discrete version of Nöther's theorem. Assuming that H inherits the symmetries of L, the integrator will *exactly* preserve the associated discrete momenta.

Second, the map is *symplectic*. Consider the discrete approximation to the action over an interval evaluated on the integrator path:

$$\mathcal{S}(q_1, q_2, \ldots, q_M) \equiv \sum_{i=1}^{M-1} H\left(h, q_i, q_i', \ldots, q_i^{(n)}, q_{i+1}\right), \quad (4)$$

where the q_i satisfy the integrator equations (2). Taking one exterior derivative of $\mathcal{S}$ gives

$$d\mathcal{S}(q_1, q_2, \ldots, q_M) = \partial_1 H\left(h, q_1, q_1', \ldots, q_1^{(n)}, q_2\right) dq_1 + \partial_{n+2} H\left(h, q_{M-1}, q_{M-1}', \ldots, q_{M-1}^{(n)}, q_M\right) dq_M; \quad (5)$$

the terms involving $dq_2, \ldots, dq_{M-1}$ are identically zero because the trajectory satisfies equations (2a), (2b) and (2c). Two exterior derivatives of $\mathcal{S}$ give zero, yielding

$$d^2\mathcal{S}(q_1, q_2, \ldots, q_M) = \partial_1\partial_{n+2} H\left(h, q_1, q_1', \ldots, q_1^{(n)}, q_2\right) dq_1 \wedge dq_2 + \partial_1\partial_{n+2} H\left(h, q_{M-1}, q_{M-1}', \ldots, q_{M-1}^{(n)}, q_M\right) dq_M \wedge dq_{M-1} = 0. \quad (6)$$

Instead of considering evolution on phase space (q, p), consider the corresponding evolution on the discrete state space (q_1, q_2). Evolution maps the initial state-space for H, $(q_1, q_2) \in \mathbb{R}^m \times \mathbb{R}^m$, to an isomorphic space, $(q_{M-1}, q_M) \in \mathbb{R}^m \times \mathbb{R}^m$, where m is the dimensionality of configuration space. Equation (6) can be written

$$\partial_1\partial_{n+2} H\left(h, q_1, q_1', \ldots, q_1^{(n)}, q_2\right) dq_1 \wedge dq_2 = F^*\left[\partial_1\partial_{n+2} H\left(h, q_1, q_1', \ldots, q_1^{(n)}, q_2\right) dq_1 \wedge dq_2\right] \quad (7)$$

using the pushforward map under evolution, F^*. All forms in equation (7) live on the cotangent bundle of the state space $\mathbb{R}^m \times \mathbb{R}^m$. We see that the integrator conserves the discrete symplectic form on the state space of H,

$$\partial_1 \partial_{n+2} H \left(h, q_1, q_1', \ldots, q_1^{(n)}, q_2 \right) dq_1 \wedge dq_2. \tag{8}$$

This is the direct analog of the symplecticity of continuous time-evolution in a Hamiltonian system.

Using equation (2a), we see that

$$-dp_1 = \partial_1 \partial_1 H(h, q_1, q', q'', \ldots, q^{(n)}, q_2) dq_1 + \partial_{n+2} \partial_1 H(h, q_1, q', q'', \ldots, q^{(n)}, q_2) dq_2, \tag{9}$$

and therefore conservation of the discrete symplectic form in equation (8) implies conservation of the Poincaré integral invariant on phase space:

$$\partial_1 \partial_{n+2} H \left(h, q_1, q_1', \ldots, q_1^{(n)}, q_2 \right) dq_1 \wedge dq_2 = dp_1 \wedge dq_1. \tag{10}$$

Finally, while it is impossible for a constant-time-stepping integrator to be momentum-conserving, symplectic and to exactly conserve energy (Ge & Marsden 1988), variational integrators generally have bounded energy error. Lew et al. (2004) explain that the discretized trajectory is sampling the continuous trajectory of a Lagrangian system, $\tilde{L}$, which is near L. $\tilde{L}$ satisfies

$$\int_{t_1}^{t_1+h} dt\, \tilde{L}(t, q(t), Dq(t)) = H \left(h, q_1, q', q'', \ldots, q^{(n)}, q_2 \right), \tag{11}$$

where the integral is evaluated on the trajectory which satisfies the Euler-Lagrange equations for $\tilde{L}$ with $q(t_1) = q_1$ and $q(t_1 + h) = q_2$ and the positions which are arguments for H satisfy equations (2). Equation (11) implies that H is the exact generating function for time evolution under $\tilde{L}$. In general it is only possible to compute a truncation of $\tilde{L}$ to any desired order in h, but it is possible to prove that $\tilde{L}$ is close to L in the space of possible Lagrangians. Since the trajectory remains on the energy level set of $\tilde{L}$ in phase space, near the energy level-set for L, the energy error remains bounded.

2.1. Galerkin Gauss-Lobatto Variational Integrators

To define a variational integrator, we need an H-type function which approximates the action for a system over an interval. There are many ways to find such a function; see Marsden & West (2001) for an extensive discussion of the various types of integrator. In

this paper, we will focus on the so-called Galerkin Gauss-Lobatto (GGL) integrators. These integrators assume a polynomial trajectory in time and approximate the action integral using a Gauss-Lobatto quadrature rule. Gauss-Lobatto quadrature is appropriate because it gives the highest-order integration rule for a given number of points subject to the constraint that the Lagrangian is evaluated once at the beginning and once at the end of the interval. Evaluating at the beginning and end of the interval is important because it preserves the symmetries of the continuous Lagrangian. Marsden & West (2001) show that all such integrators can be written as symplectic partitioned Runge-Kutta integrators and derive formulas which relate the SPRK coefficients to the discrete Lagrangian.

We define

$$\begin{aligned} H(h, q_1, q', \ldots, q^{(n)}, q_2) \equiv\ & w_1 L(t_1, \phi(t_1, q_1, q', \ldots, q^{(n)}, q_2, t_1, h), \partial_0\phi(t_1, q_1, q', \ldots, q^{(n)}, q_2, t_1, h)) \\ & + \sum_{i=1}^{n} w^{(i)} L(t^{(i)}, \phi(t^{(i)}, q_1, q', \ldots, q^{(n)}, q_2, t_1, h), \partial_0\phi(t^{(i)}, q_1, q', \ldots, q^{(n)}, q_2, t_1, h)) \\ & + w_2 L(t_1 + h, \phi(t_1 + h, q_1, q', \ldots, q^{(n)}, q_2, t_1, h), \partial_0\phi(t_1 + h, q_1, q', \ldots, q^{(n)}, q_2, t_1, h)), \quad (12) \end{aligned}$$

where $\phi(t, q_1, q', \ldots, q^{(n)}, q_2, t_1, h)$ is the interpolating polynomial for $q(t)$ passing through the points $\{q_1, q', \ldots, q^{(n)}, q_2\}$ at times $\{t_1, t', \ldots, t^{(n)}, t_1 + h\}$. The times $\{t_1, t', \ldots, t^{(n)}, t_1 + h\}$ and weights $\{w_1, w', \ldots, w^{(n)}, w_2\}$ define the $n+2$ point Gauss-Lobatto quadrature rule. This rule is exact for quadrature of polynomials up to and including order $2n+2$. The integrator so defined will be of order $2n + 2$. See, for example, Abramowitz & Stegun (1972, Table 25.6) for appropriate times and weights. This is easier than it looks; examples follow.

2.1.1. Two-Point Integrator

The two-point Gauss-Lobatto integration rule has times $\{t_1, t_1+h\}$ and weights $\{h/2, h/2\}$; a two-point interpolating polynomial is a line. Therefore, we have

$$H(h, q_1, q_2) = \frac{h}{2}\left[L\left(t_1, q_1, \frac{q_2 - q_1}{h}\right) + L\left(t_1 + h, q_2, \frac{q_2 - q_1}{h}\right)\right]. \quad (13)$$

For a Lagrangian $L(t, q, v) = \frac{1}{2}mv^2 - V(q)$, equations (2a) and (2c) result in the explicit integration rule

$$q_2 = q_1 + h\frac{p_1}{m} - \frac{h^2}{2m}DV(q_1) \quad (14a)$$

$$p_2 = m\frac{q_2 - q_1}{h} - \frac{h}{2}DV(q_2). \quad (14b)$$

This rule is kick-drift-kick leapfrog; it can be derived from the Hamiltonian viewpoint by iterating the evolutions of the splitting of the Hamiltonian for this system into $H_1(q,p) = V(q)$ and $H_2(q,p) = p^2/(2m)$ (for a thorough exploration of this idea see, for example, Wisdom & Holman (1991) and Yoshida (1993)). This rule is second order, as expected from the order of the quadrature rule.

2.1.2. Three-Point Integrator

The three-point Gauss-Lobatto quadrature rule has times $\{t_1, t_1 + h/2, t_1 + h\}$ and weights $\{h/6, 2h/3, h/6\}$. The three-point interpolation polynomial is quadratic in time. Applying equation (12), we find

$$H(h,q_1,q',q_2) = h\left[\frac{1}{6}L\left(t_1,q_1,\frac{4q'-3q_1-q_2}{h}\right)\right.$$
$$\left.+\frac{2}{3}L\left(t_1+\frac{h}{2},q',\frac{q_2-q_1}{h}\right)+\frac{1}{6}L\left(t_1+h,q_2,\frac{q_1+3q_2-4q'}{h}\right)\right]. \quad (15)$$

If $L(t,q,v) = \frac{1}{2}mv^2 - V(q)$ then equations (2a), (2b) and (2c) reduce to

$$q' = q_1 + \frac{h}{2}\frac{p_1}{m} - \frac{h^2}{12m}DV(q_1) - \frac{h^2}{24m}DV(q') \quad (16a)$$

$$q_2 = 8q' - 7q_1 - 3h\frac{p_1}{m} + \frac{h^2}{2m}DV(q_1) \quad (16b)$$

$$p_2 = \frac{m}{3h}(q_1 - 8q' + 7q_2) - \frac{h}{6}DV(q_2). \quad (16c)$$

To implement this integration scheme, we must solve the implicit equation (16a) for q'. In spaces of high dimensionality (i.e. an N-body system with large N), the only efficient way to do this is through iteration: we treat equation (16a) as a prescription for updating the value of q', and iterate.

The iteration generates a sequence of middle-points, $q', q'', \ldots, q^{(k)}$. Each element of the sequence is related to the prior element by

$$q^{(i+1)} = q_1 + \frac{h}{2}\frac{p_1}{m} - \frac{h^2}{12m}DV(q_1) - \frac{h^2}{24m}DV\left(q^{(i)}\right). \quad (17)$$

The quantity $\Delta^{(i)}$, defined by

$$\Delta^{(i)} \equiv q^{(i)} - \left[q_1 + \frac{h}{2}\frac{p_1}{m} - \frac{h^2}{12m}DV(q_1) - \frac{h^2}{24m}DV\left(q^{(i)}\right)\right], \quad (18)$$

measures how well equation (16a) is satisfied by $q^{(i)}$. Because the proofs of momentum conservation and symplecticity rely on the trajectory exactly satisfying equations (16a), (16b), and (16c), the non-conservation of momentum and non-symplecticity are proportional to

$$\partial_2 H\left(h, q_1, q^{(i)}, q_2\right) \propto \frac{\Delta^{(i)}}{h} \tag{19}$$

if we stop the sequence with $q^{(i)}$. Iterating to convergence drives $\Delta^{(i)} \to 0$, whence equation (16a) is exactly satisfied. Using equation (17), we can estimate $\Delta^{(i)}$ as

$$\begin{aligned}\Delta^{(i)} &= \frac{h^2}{24m}\left[DV\left(q^{(i)}\right) - DV\left(q^{(i-1)}\right)\right] \\ &\approx \frac{h^2}{24m}\left[\left(q^{(i)} - q^{(i-1)}\right) D^2V\left(q^{(i)}\right)\right] \sim \mathcal{O}\left(h^2\left(q^{(i)} - q^{(i-1)}\right)\right),\end{aligned} \tag{20}$$

where the last relation follows because $D^2V(q)$ does not depend on the stepsize h. Thus, the error in symplecticity and momentum conservation scales one power of h better than the correction to $q^{(i-1)}$ from equation (17) over a single step, and scales as the same power of h over a fixed time interval. The correction to $q^{(i-1)}$ is

$$\begin{aligned}q^{(i)} - q^{(i-1)} &= \frac{h^2}{24m}\left[DV\left(q^{(i-2)}\right) - DV\left(q^{(i-1)}\right)\right] \\ &\approx \frac{h^2}{24m}\left[\left(q^{(i-2)} - q^{(i-1)}\right) D^2V\left(q^{(i-1)}\right)\right] \sim \mathcal{O}\left(h^2\left(q^{(i-1)} - q^{(i-2)}\right)\right).\end{aligned} \tag{21}$$

We see that the correction to $q^{(i-1)}$ decreases by h^2 every iteration. This implies that the order of the symplecticity and momentum conservation error increases by two every iteration of equation (17) *even though the trajectory error never scales better than* h^4.

The number of iterations of equation (17) required to reach a specified accuracy in symplecticity and momentum conservation depends on the initial prediction for q'. The simplest such prediction is

$$q' = q_1 + \frac{p_1}{m}\frac{h}{2} = q\left(\frac{h}{2}\right) + \mathcal{O}\left(h^2\right). \tag{22}$$

Then the first application of equation (17) results in $q'' - q' \sim \mathcal{O}\left(h^2\right)$ and the second in $q''' - q'' \sim \mathcal{O}\left(h^4\right)$, at which point we have a fourth-order integrator with fourth order non-conservation of momentum and symplecticity.

It is possible to do much better, however. Given that the integration method requires calculating potential gradients at t, $t + h/2$, and $t + h$ we can fit the resulting forces to a

polynomial in time and compute $F(t)$, $DF(t)$, and $D^2F(t)$ with negligible work using the polynomial fit to the last step's forces. Then the predictor

$$q' = q_1 + \frac{p_1}{m}\frac{h}{2} + \frac{F(t)}{2m}\left(\frac{h}{2}\right)^2 + \frac{DF(t)}{6m}\left(\frac{h}{2}\right)^3 + \frac{D^2F(t)}{24m}\left(\frac{h}{2}\right)^4 = q\left(t+\frac{h}{2}\right) + \mathcal{O}\left(h^5\right), \quad (23)$$

results in $q''-q' \sim \mathcal{O}\left(h^5\right)$ after a single application of equation (17)—a fourth-order integrator in trajectory error with fifth order momentum conservation and symplecticity over fixed integration time. Note that the "first step same as last step" property of this integrator means that, for long runs, the number of potential evaluations per step asymptotes to 2—that is, it is a fourth-order scheme with fifth-order symplecticity and momentum-conservation errors with only two potential evaluations per step. This is the approach we will use for the individual and adaptive timestep integrator described in Section 5. With a shared timestep h, nothing prevents us from iterating equation (17) more times to improve the symplecticity and momentum-conservation error. Each additional potential evaluation in equation (17) obtains an extra h^2 in these errors (but not in the trajectory error).

The three-point GGL integrators take only forward steps in time. It is not possible to write these integrators as iterated evolution of a split Hamiltonian (as in the two-point case): a general theorem states that it is impossible to have evolution by Hamiltonian splitting which is higher than second-order accurate and takes only forward steps (Suzuki 1991; Sheng 1989). It is possible to formulate higher-order mapping integrators from the Hamiltonian perspective which take only forward steps using the *force* gradient (Wisdom et al. 1996; Scuro & Chin 2005; Chin & Chen 2003), but force gradients can be very expensive to compute. Forward time steps are important for cosmological simulations which include gas dynamics because such simulations are unstable under time reversal. The requirement of symplecticity and forward timesteps has previously restricted cosmological simulations to second-order mapping integrators (Springel 2005a).

It is straightforward to derive the integration equations for $n+2$-point GGL integrators with $n > 1$. All such integrators have implicit equations for the intermediate positions, $q', \ldots, q^{(n)}$, which must be solved via iteration exactly as in the $n = 1$ case discussed above. In the presence of individual timesteps, we must predict the middle positions and apply the iteration only once, as will be explained below. For an $n+2$-point GGL the predictor analogous to equation (23) has an error term which is $\mathcal{O}\left(h^{n+4}\right)$, and therefore the momentum and symplecticity error are also $\mathcal{O}\left(h^{n+4}\right)$ after a single iteration. But, the integrator itself has a best-case trajectory error of $\mathcal{O}\left(h^{2n+2}\right)$; this error is limited by the order of the Gauss-Lobatto quadrature rule used. Only for the case $n = 1$ (the three-point GGL integrator) does the bound on momentum and symplecticity error exceed the bound on trajectory error. For $n > 1$, GGL integrators conserve momentum and the Poincaré integral invariant at the same

order as their trajectory error—there is no error-scaling benefit to the variational approach over any other type of integrator of the same order of trajectory error. For this reason, we do not consider $n+2$-point GGL integrators with $n > 1$ in this paper.

3. Adaptive Timesteps

In N-body simulations it is essential to be able to adapt the timestep taken by an integrator to the local conditions of the system. Formally, we can model such an adaptive step by treating the parameter h in the discrete Lagrangian describing an integrator as a function of the positions through the step:

$$H\left(h, q_1, q_1', \ldots, q_1^{(n)}, q_2\right) \rightarrow H\left(h\left(q_1, q_1', \ldots, q_1^{(n)}, q_2\right), q_1, q_1', \ldots, q_1^{(n)}, q_2\right). \tag{24}$$

Because the sequence of positions $q_1, q_1', \ldots, q_1^{(n)}, q_2$ encodes all available information about the trajectory, essentially *any* technique for choosing a timestep can be recast in this fashion. We do not change the integrator equations

$$\partial_1 H\left(h\left(q_1, q_1', \ldots, q^{(n)}, q_2\right), q_1, q_1', \ldots, q_1^{(n)}, q_2\right) = -p_1 \tag{25}$$

$$\partial_i H\left(h\left(q_1, q_1', \ldots, q^{(n)}, q_2\right), q_1, q_1', \ldots, q_1^{(n)}, q_2\right) = 0, \qquad i = 2, 3, \ldots, n+1 \tag{26}$$

$$\partial_{n+2} H\left(h\left(q_1, q_1', \ldots, q^{(n)}, q_2\right), q_1, q_1', \ldots, q_1^{(n)}, q_2\right) = p_2. \tag{27}$$

Assuming that the timestep function $h\left(q_1, q_1', \ldots, q_1^{(n)}, q_2\right)$ is invariant under the same coordinate variations which leave H invariant (this will be the case if both H and h inherit the same symmetries from the continuous Lagrangian), then the proof of momentum conservation in equation (3) still holds. All terms in δH proportional to $\partial_0 H\left(h\left(q_1, q_1', \ldots, q_1^{(n)}, q_2\right), q_1, q_1', \ldots, q_1^{(n)}, q\right.$ vanish because δh also vanishes. Adaptive stepping poses no threat to momentum conservation, provided that the steps are chosen in a way which respects the symmetries in the continuous mechanical problem.

Unfortunately, adaptive stepping does pose a threat to symplecticity. With a timestep

function $h\left(q_1, q_1', \ldots, q_1^{(n)}, q_2\right)$, the expression for $d\mathcal{S}$ (see eq. (5)) gets additional terms:

$$\sum_{i=1}^{M-1} \partial_0 H\left(h\left(q_i, q_i', \ldots, q_i^{(n)}, q_{i+1}\right), q_i, q_i', \ldots, q_i^{(n)}, q_{i+1}\right) \left[\partial_0 h\left(q_i, q_i', \ldots, q_i^{(n)}, q_{i+1}\right) dq_i + \sum_{j=1}^{n} \partial_j h\left(q_i, q_i', \ldots, q_i^{(n)}, q_{i+1}\right) dq_i^{(j)} + \partial_{n+1} h\left(q_i, q_i', \ldots, q_i^{(n)}, q_{i+1}\right) dq_{i+1}\right]. \quad (28)$$

These extra terms prevent us from writing $d^2\mathcal{S} = 0$ as the difference of two forms, one of which is the pushforward of the other, as we did in equation (7). With general adaptive timesteps, there is no two-form on the state space which is conserved over a fixed number of steps.

This can be understood intuitively in the following way. Symplecticity is the conservation of the Poincaré integral invariant

$$\mathcal{I} \equiv \sum_i dq^i \wedge dp_i, \quad (29)$$

with the sum taken over coordinate dimensions, along any trajectory (recall that eq. (10) shows that conservation of the two-form $\partial_1 \partial_{n+2} H\left(h, q_1, q_1', \ldots, q_1^{(n)}, q_2\right) dq_1 \wedge dq_2$ on state space implies conservation of $\mathcal{I}$ on phase space). Note that dq^i and dp_i are exterior derivatives and that $\mathcal{I}$ is a two-form. The Poincaré integral invariant measures the sum of the areas of a tube of trajectories infinitesimally near a reference trajectory projected onto the sub-phase-spaces (q^i, p_i). But an integrator with an adaptive timestep does not advance all trajectories in the tube with the same h. Even if we had an adaptive timestep integrator which implemented the exact, continuous evolution of the system it still would not conserve $\mathcal{I}$ over a single step—stopping the evolution of the different trajectories in the tube at different times spoils the symplecticity of the continuous evolution. For an adaptive timestep integrator symplecticity after a fixed number of steps *is the wrong condition to consider*. Rather, we should ask whether the integrator conserves the symplectic form over a fixed total time of evolution. In general, any well-behaved[1] integrator (including a variational integrator with general adaptive stepsizes) which has trajectory error of order h^r conserves the symplectic form to order h^r in this sense.

[1]In this case, "well-behaved" implies an integrator whose maps converge uniformly at order h^r to the exact evolution map and whose derivatives converge uniformly as well.

For variational integrators which choose timesteps using the popular block-power-of-two scheme we can do better: these integrators conserve the symplectic form almost everywhere in phase space. In the block-power-of-two scheme, a function $h_{\max}\left(q_1, q_1', \ldots, q_1^{(n)}, q_2\right)$ limits the maximum timestep; the actual timestep taken is rounded down from h_{max} to the nearest number of the form $T/2^n$, with n an integer, and T some total evolution interval. If the function h_{max} is continuous, about every point in state space for which $h_{\max}\left(q_1, q_1', \ldots, q_1^{(n)}, q_2\right) \neq T/2^n$ for some n there is an open neighborhood of points which round down to the same timestep. Thus, the actual timestep function $h\left(q_1, q_1', \ldots, q_1^{(n)}, q_2\right)$ is piecewise-constant on state space, and the derivatives in equation (28) vanish almost everywhere on state space for each step. A variational integrator with adaptive block-power-of-two timesteps is therefore symplectic almost everywhere on state space because it is a composition of symplectic steps. ("Almost everywhere" should be taken in the mathematical sense of "except on a set of measure zero.") In Section 6 we present numerical evidence of this phenomenon. Incidentally, block-power-of-two timesteps have advantages for parallelization which have led other authors to adapt time-symmetric methods to block-power-of-two timesteps (Makino et al. 1996). Variational integrators fit naturally into a block-power-of-two scheme which, in addition to its ease of parallelization, preserves symplecticity in the presence of adaptive timesteps.

All adaptive timestep integrators discussed in the remainder of this paper use block-power-of-two timestep schemes.

4. Individual Time Steps

Astrophysical simulations of realistic systems often require individual time steps for each body or for subgroups of bodies. A variation of the three-point GGL integrator described in Section 2.1.2 allows for individual steps.

It is instructive to consider the introduction of individual timesteps in the integrators presently in use. Large-scale cosmological simulations use either kick-drift-kick leapfrog (the 2-point GGL integrator from Section 2.1.1) or drift-kick-drift leapfrog (Springel 2005b; Shirokov & Bertschinger 2005). Either case is an operator splitting of the N-body Hamiltonian into kinetic terms (which generate the drift) and potential terms (which generate the kicks). The integrator is a composition of drift and kick evolutions. Individual timesteps can be assigned to each term in the potential, resulting in a sub-cycling of kick operators. This approach will not work for GGL integrators other than the two-point because they cannot be written as a composition of separate evolution operators.

Cluster simulations generally use the Hermite integration scheme (Makino 1991), which is a predictor-corrector integrator. Predictor-corrector integrators assign a timestep to each body and use a predictor to estimate the position of the body at arbitrary times within its timestep; these intermediate positions are required to evaluate the force between bodies at arbitrary times. Forces on each body are accumulated through that body's timestep, and then used to correct the predicted final position of the body. This is the approach we will use for the GGL three-point integrator.[2]

Write the N-body Lagrangian as a sum over particle indices $i = 1 \ldots N$:

$$L = \sum_{i=1}^{N} \left[\frac{m^i}{2} \left(Dq^i(t) \right)^2 - \sum_{j=i+1}^{N} m^i m^j V \left(q^i(t) - q^j(t) \right) \right], \tag{30}$$

where $V(q) = -1/|q|$ (recall we suppress vector indices). Assume for the moment that the timesteps of each body, h^i, are fixed in time (Section 5 discusses how to integrate adaptive steps into this algorithm), and that particles are sorted so that $h^i \leq h^j$ when $i < j$. Let $n^i = \Delta t / h^i$ be the number of timesteps of body i over the integration interval Δt; for simplicity, we assume the integration starts at time $t = 0$ and finishes at time $t = \Delta t$. Then we can write an approximation to the action S over that interval using the three-point Gauss-Lobatto quadrature rule as

$$\begin{aligned} S \approx \sum_{i=1}^{N} \sum_{k=0}^{n^i - 1} h^i \Bigg[\frac{m^i}{2} \Bigg(& \frac{\left[Dq^i \left(k h^i \right) \right]^2}{6} + \frac{2 \left[Dq^i \left(\frac{2k+1}{2} h^i \right) \right]^2}{3} + \frac{\left[Dq^i \left((k+1) h^i \right) \right]^2}{6} \Bigg) \\ & - \frac{m^i}{6} \sum_{j=i+1}^{N} m^j V \left(q^i \left(k h^i \right) - q^j \left(k h^i \right) \right) \\ & - \frac{2 m^i}{3} \sum_{j=i+1}^{N} m^j V \left(q^i \left(\frac{2k+1}{2} h^i \right) - q^j \left(\frac{2k+1}{2} h^i \right) \right) \\ & - \frac{m^i}{6} \sum_{j=i+1}^{N} m^j V \left(q^i \left((k+1) h^i \right) - q^j \left((k+1) h^i \right) \right) \Bigg]. \end{aligned} \tag{31}$$

Figure 1 illustrates the series of potential evaluations in the above expression assuming, for graphical simplicity, that $h^j = 2^{j-1} h^1$.

---

[2]In Hut & Makino (2006, Maya, Chapter 12, Section 1.2) the authors assert that no individual timestep Runge-Kutta integrator exists for use in astrophysics. By Marsden & West (2001, Theorem 2.6.2) all GGL variational integrators can be written as symplectic partitioned Runge-Kutta integrators, so the integrator described in this paper would be the first.

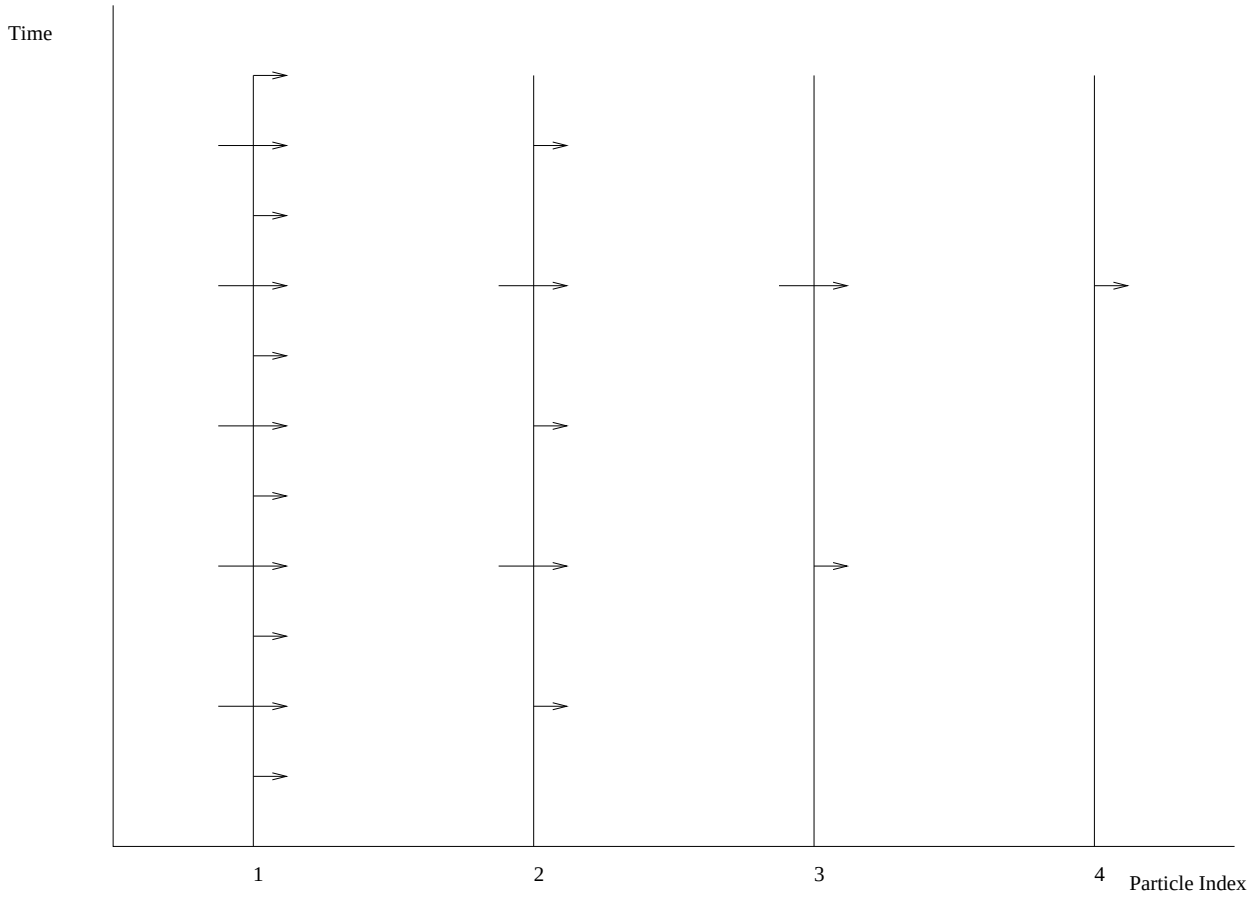

Fig. 1.— Time-sequence of potential evaluations in the integral approximation to the action, equation (31), assuming, for graphical simplicity, that $h^j = 2^{j-1}h^1$. Time runs vertically and particle index runs horizontally. A right-facing arrow crossing a particle timeline represents evaluation of potentials involving that particle and all particles of greater index. Long arrows represent evaluations of potentials at the beginning and end of particle timesteps (associated with coefficients $h/6$); short arrows represent evaluations of potentials at particle half-timesteps (with coefficient $2h/3$).

We give each particle a discretized trajectory parameterized on timestep k by

$$q_k^i \equiv q^i\left(kh^i\right) \quad q_k'^i \equiv q^i\left(\frac{2k+1}{2}h^i\right) \quad q_{k+1}^i \equiv q^i\left((k+1)h^i\right). \tag{32}$$

Let $l_j(t)$ be the integer such that $l_j(t)h^j \leq t < (l_j(t)+1)\,h^j$. At time t, particle number j is on step $l_j(t)$. Using the interpolated trajectories, we can write the action approximation as

$$\begin{aligned} S \approx \sum_{i=1}^{N}\sum_{k=0}^{n^i-1} h^i \Bigg[& \frac{7\left(q_k^i\right)^2 + 16\left(q_k'^i\right)^2 + 7\left(q_{k+1}^i\right)^2 - 16q_k'^i q_{k+1}^i + 2q_k^i\left(q_{k+1}^i - 8q_k'^i\right)}{3h^2} \\ & - \frac{m^i}{6}\sum_{j=i+1}^{N} m^j V\left(q_k^i - \phi\left(kh^i, q^j_{l_j(kh^i)}, q'^j_{l_j(kh^i)}, q^j_{l_j(kh^i)+1}, l_j(kh^i)h^j, h^j\right)\right) \\ & -\frac{2m^i}{3}\sum_{j=i+1}^{N} m^j V\left(q_k'^i - \phi\left(\frac{2k+1}{2}h^i, q^j_{l_j\left(\frac{2k+1}{2}h^i\right)}, q'^j_{l_j\left(\frac{2k+1}{2}h^i\right)}, q^j_{l_j\left(\frac{2k+1}{2}h^i\right)+1}, l_j(\frac{2k+1}{2}h^i)h^j, h^j\right)\right) \\ & -\frac{m^i}{6}\sum_{j=i+1}^{N} m^j V\left(q_{k+1}^i - \phi\left((k+1)h^i, q^j_{l_j((k+1)h^i)}, q'^j_{l_j((k+1)h^i)}, q^j_{l_j((k+1)h^i)+1}, l_j\left((k+1)h^i\right)h^j, h^j\right)\right)\Bigg], \end{aligned} \tag{33}$$

where $\phi(t, q_0, q_1, q_2, t_0, h)$ is the value of the unique polynomial passing through $\{q_0, q_1, q_2\}$ at times $\{t_0, t_0 + h/2, t_0 + h\}$ at time t.

The action approximation in equation (33) only couples the triples of points $q_k^i, q_k'^i, q_{k+1}^i$ for all particles i and timesteps k. Thus, we can write an H-type function for each particle

i's timestep k:

$$H_k^i\left(h^i, q_k^i, q_k'^i, q_{k+1}^i\right) = h^i \left[\frac{7\left(q_k^i\right)^2 + 16\left(q_k'^i\right)^2 + 7\left(q_{k+1}^i\right)^2 - 16 q_k'^i q_{k+1}^i + 2 q_k^i\left(q_{k+1}^i - 8 q_k'^i\right)}{3h^2}\right.$$
$$- \frac{m^i}{6}\sum_{j=i+1}^{N} m^j V\left(q_k^i - \phi\left(kh^i, q_{l_j(kh^i)}^j, q_{l_j(kh^i)}'^j, q_{l_j(kh^i)+1}^j, l_j(kh^i)h^j, h^j\right)\right)$$
$$- \frac{2m^i}{3}\sum_{j=i+1}^{N} m^j V\left(q_k'^i - \phi\left(\frac{2k+1}{2}h^i, q_{l_j(kh^i)}^j, q_{l_j(kh^i)}'^j, q_{l_j(kh^i)+1}^j, l_j(kh^i)h^j, h^j\right)\right)$$
$$\left. - \frac{m^i}{6}\sum_{j=i+1}^{N} m^j V\left(q_{k+1}^i - \phi\left((k+1)h^i, q_{l_j(kh^i)}^j, q_{l_j(kh^i)}'^j, q_{l_j(kh^i)+1}^j, l_j(kh^i)h^j, h^j\right)\right)\right]$$
$$- m^i \sum_{j=1}^{i-1} h^j \left[\frac{m^j}{6}\sum_{\{p\,|\,l_i(ph^j)=k\}} V\left(q_p^j - \phi\left(ph^j, q_k^i, q_k'^i, q_{k+1}^i, kh^i, h^i\right)\right)\right.$$
$$+ \frac{2m^j}{3}\sum_{\{p\,|\,l_i((2p+1)h^j/2)=k\}} V\left(q_p'^j - \phi\left(\frac{2p+1}{2}h^j, q_k^i, q_k'^i, q_{k+1}^i, kh^i, h^i\right)\right)$$
$$\left. + \frac{m^j}{6}\sum_{\{p\,|\,l_i((p+1)h^j)=k\}} V\left(q_{p+1}^j - \phi\left((p+1)h^j, q_k^i, q_k'^i, q_{k+1}^i, kh^i, h^i\right)\right)\right]. \quad (34)$$

The potential evaluations in this expression are represented graphically in Figure 2.

Implementing equations (2a), (2b) and (2c) for the H in equation (34) requires differentiating H with respect to q_k^i, $q_k'^i$, and q_{k+1}^i. This gives equations exactly like (16a), (16b) and (16c) except with a sum over potential terms. For potential terms which involve an interpolation over the positions of particle i, the force $-DV$ is multiplied by the interpolation coefficient for the corresponding points in equations (16a), (16b) and (16c) (because ϕ is linear in the interpolated positions). Heuristically, we can imagine that each particle has three force bins, corresponding to derivatives with respect to the three positions. Forces are distributed into the bins throughout the particle's step according to the interpolation coefficients as the potential terms are evaluated. At the end of the step, the final position and momentum are calculated using equations (16a), (16b) and (16c), substituting the accumulated forces for $-DV$ in the equations. Because both body i and body j receive the contribution from evaluating potential $V\left(q^i - q^j\right)$ at the same time, this integrator will exactly conserve linear momentum notwithstanding the discussion in Section 2.1.2. Conservation of other momenta associated with symmetries (i.e. angular momentum) will be fifth-order.

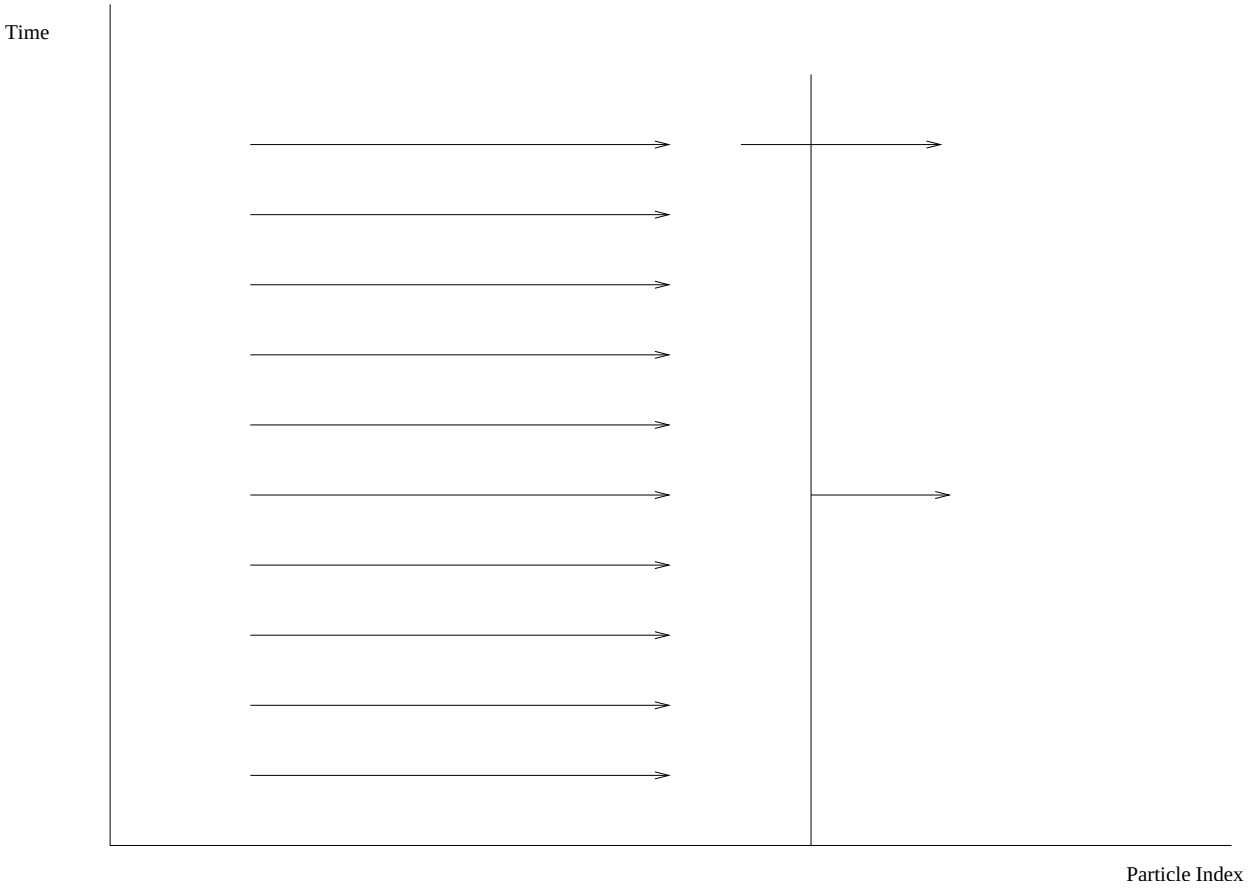

Fig. 2.— Graphical representation of the time-sequence of potential evaluations in equation (34). Time runs vertically and particle index horizontally; we are focusing on the terms in H_k^i—the potential terms involving particle i on its kth timestep. The arrows coming from the left represent evaluations of potentials between particle i and particles j with $j < i$. Because these particles have smaller timesteps than particle i these potentials are evaluated many times over a single step of particle i. At most of these evaluations, the position of particle i must be interpolated using its predicted positions at the start, middle and end of its timestep—hence the ϕ terms for particle i in equation (34). The arrows to the right represent the three evaluations of potentials between particle i and particles j with $j > i$. Because these potentials are evaluated exactly at the beginning, middle, and end of i's step, no interpolation on i's position is necessary (the ϕ in these terms in equation (34) involves the positions of particle j).

5. Adaptive Stepping and Individual Block Power of Two Timesteps

In this section we combine the block-power-of-two adaptive timesteps described in Section 3 with the individual timestep algorithm described in Section 4. In order that the discrete Lagrangian, equation (33), approximate the action for the N-body system, we require $h^i \leq h^j$ for $i < j$. Thus, changing the timestep for a body potentially requires re-ordering the sum in equation (33). Bodies i and j can only change relative position in the sum when *both* have finished a step, or there will be some potentials whose evaluations in the discrete Lagrangian do not correspond to a proper Gauss-Lobatto quadrature rule. Using block-power-of-two timesteps,

$$h^i = \frac{\Delta t}{2^{p^i}}, \quad p^i = 1 \text{ or } 2 \text{ or } 3, \ldots, \tag{35}$$

for some total integration interval Δt. With block-power-of-two timesteps, all bodies completing a timestep at a given time are contiguous in the sum from indices 1 to some $i^{\max}$. We can re-compute the maximum timestep allowable for each of these bodies and sort them in the sum according to their maximum timestep. Once the maximum timesteps are calculated, we must ensure that the actual timesteps taken satisfy

$$h^i \leq \min\left(h^i_{\max}, h^{i^{\max}+1}\right), \quad i = 1, 2, \ldots, i^{\max}, \tag{36}$$

subject to the power-of-two restrictions in equation (35). This procedure preserves the invariant that $h^i < h^j$ for $i < j$ and ensures $h^i < h^i_{\max}$.

Makino (1991) recommends choosing a timestep which reflects the error of the predictor relative to the final solution. We choose

$$h^i_{\max} = h^i \left(\frac{\eta \left(h^i\right)^2 F}{m \left| q^i - q^i_{\text{pred}} \right|} \right)^{1/5} \tag{37}$$

where η is an accuracy parameter of the simulation, and q^i_{pred} is the predicted position of the particle using equation (23), while q^i is the position as determined by the integrator at the end of the prior timestep. The exponent is $1/5$ because the integrator is $O(h^4)$.

The complete algorithm to advance body i by dt, assuming an array of bodies sorted by h_{max} and indexed from 0 to $N-1$ is then:

1. If $dt \leq h^i_{\max}$ then

   (a) Predict the positions of body i at $t + dt/2$ and $t + dt$ using equation (23).

(b) Compute potential gradients between body i and bodies j, with $j > i$, at times t, $t+dt/2$, and $t+dt$, distributing the forces across the force bins of body j according to the interpolation coefficients for the position of body j at these times. Also accumulate the force into the corresponding bin of body i.

(c) Unless $i = 0$, advance body $i-1$ by dt. Note that upon completion of this step the force on body i from all bodies with indices below i will be stored in i's bins.

(d) Update the position of body i using equations (16a), (16b), and (16c). Calculate a new $h^i_{\max}$.

2. Otherwise

(a) Advance body i by $dt/2$.

(b) Sort bodies 0 to i according to their maximum timesteps.

(c) Advance the body at index i (which may not be the same body after the sort) by $dt/2$.

The algorithm begins by attempting to advance body $N-1$ by the entire time interval, Δt. The order of computations and recursion above ensures that the timesteps are block-power-of-two, that the total integration terminates after advancing the bodies by exactly Δt, and maintains the invariant that $h^i \leq h^j$ when $i < j$.

6. Numerical Experiments

In this section we report on numerical experiments involving two different GGL variational integrators. The first integrator solves for one-dimensional Keplerian orbits using the evolution mapping defined by equations (16) and the standard Kepler Lagrangian; the second is a general N-body integrator using the adaptive-stepsize, individual timestep algorithm described above. The source code for both integrators is available upon request.

6.1. One-Dimensional Simulation

To illustrate the energy conservation and symplecticity performance of adaptive and non-adaptive variational integrators, we performed several one-dimensional simulations of the Kepler problem,

$$L(r, v) = \frac{mv^2}{2} - \frac{l^2}{2mr^2} + \frac{k}{r}. \tag{38}$$

The particular parameters we chose were $m = k = 2/9$, and $l = 2\sqrt{19}/135$, with initial conditions $r_0 = 2/45$, $v_0 = p_0 = 0.0$. With these parameters and initial conditions the total energy of the system is $E = -1/4$, the eccentricity is $e = 9/10$, and the orbital period is $\tau = 2\pi\,(2/45)^{3/2} \approx 0.0588716$. We evolved the system for various times, from $\tau/10$ to 10τ in increments of $\tau/10$. The plots shown in Figures 3 and 4 use values computed at the end of a simulation over the appropriate total time interval, not snapshots of the corresponding values in an ongoing simulation; the distinction is important because of what it implies about the choices of adaptive timesteps—see Section 3. We used three different integration algorithms based on equations (16): a constant timestep integrator, an adaptive timestep integrator where h is chosen at the beginning of a step according to

$$h(q,p) = \eta \left(\frac{mq^3}{k}\right)^{1/2}, \tag{39}$$

where $q = r$ and we set $\eta = 0.05$, and finally we used a block-power-of-two timestep integrator which uses the above for its h_{max}. For the constant timestep integrator, we chose the timestep $h\,(r_0, p_0)$. All algorithms iterate equation (16a) to convergence; we thus expect the block-power-of-two and constant timestep algorithms to be exactly symplectic.

Figure 3 displays the relative energy error accumulated over many simulated orbits by the three algorithms. It is clear that the three algorithms accumulate comparable energy error, with the adaptive timestep choice slightly worse than the others.

Given an evolution mapping $F_t : (q,p) \mapsto (Q_t(q,p), P_t(q,p))$, the pushforward of the Poincaré integral invariant $\mathcal{I} \equiv dq \wedge dp$ along the trajectory $q(t), p(t) = F_t\,(q_0, p_0)$ is given by

$$\left(F_t^* \mathcal{I}\right)(q_0,p_0) = \left[\partial_0 Q_t\,(q_0,p_0)\,\partial_1 P_t\,(q_0,p_0) - \partial_1 Q_t\,(q_0,p_0)\,\partial_0 P_t\,(q_0,p_0)\right] dq_0 \wedge dp_0. \tag{40}$$

All three integration algorithms are evolution mappings. An elegant algorithm (Sussman 2006; Sussman et al. 2001) exists to compute derivatives of arbitrary computations, such as our evolution mappings, without the truncation error which would result from finite differencing. We used this algorithm to compute $\left[\left(F_t^* \mathcal{I}\right) - \mathcal{I}\right](q_0, p_0)$ using equation (40); the results are plotted versus t for the three algorithms in Figure 4. It is clear that the ordinary adaptive stepsize integrator does not conserve the symplectic form while the block-power-of-two and constant stepsize integrators do, as expected from Section 3. As explained in Section 3, though the energy error performance of the three algorithms is comparable, only the constant-timestep and block-power-of-two schemes are symplectic, and only the block-power-of-two scheme is symplectic *and* allows for adaptive timesteps.

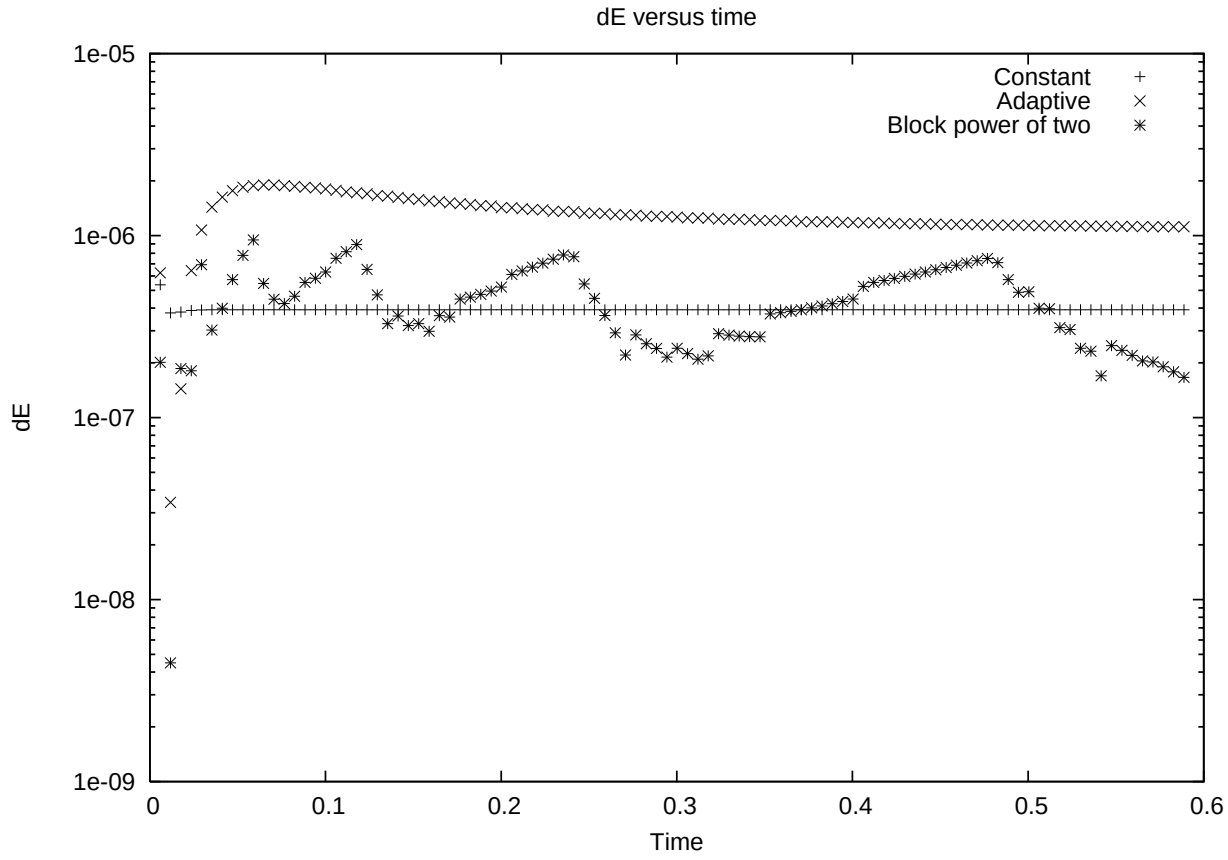

Fig. 3.— Relative energy error versus total evolution interval for simulations of the Kepler orbit described in the text. The orbital parameters are $a = 2/45$, $e = 9/10$, $E = -1/4$. The total evolution interval for each simulation varies from $\tau/10$ to 10τ in steps of $\tau/10$. All three integration algorithms have comparable energy error, but the two adaptive methods run approximately twice as fast as the constant-timestep method.

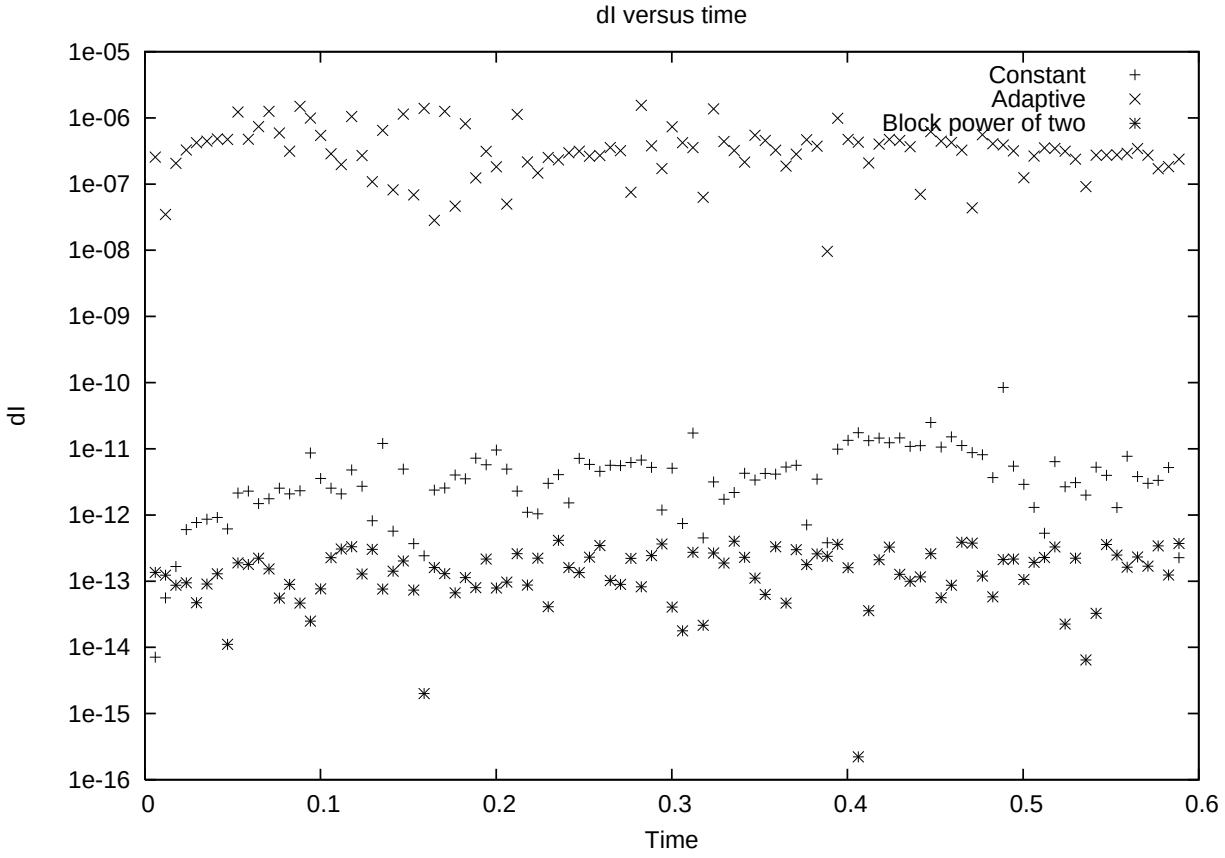

Fig. 4.— Error in the Poincaré integral invariant versus total evolution interval for the simulations of the Kepler orbit shown in Figure 3. The constant timestep and block-power-of-two timestep algorithms conserve the Poincaré integral invariant while the adaptive timestep algorithm doesn't, even though the energy error behaviors of the algorithms are comparable.

6.2. Many-Body Simulations

In this subsection we report on the application of the individual and adaptive timestep integration algorithm described in this paper to simulations of many-body systems. We choose to use the so-called "standard units": units in which the total system mass $M = 1$, $G = 1$, and the total energy $E = -1/4$ (Heggie & Mathieu 1986). In standard units, the virial radius of the system is 1. Our initial conditions are a randomly sampled Plummer model shifted into a coordinate system where the center of mass is at the origin and the total linear momentum is zero.

Because our code makes no special provision for close encounters, we used a softened gravitational potential:

$$V(r) = \frac{1}{\sqrt{r^2 + \epsilon^2}}, \tag{41}$$

with $\epsilon = 4/N$, where N is the number of bodies in a particular simulation. This is a standard technique in codes which do not carefully regularize the singular two-body potential (Aarseth 2001).

6.2.1. Symplecticity Tests

An N-body system with N bodies has a $6N$-dimensional phase space. Given an integration mapping, with Jacobian matrix J, conservation of the Poincaré integral invariant by the mapping implies that

$$S = J^T S J, \tag{42}$$

where S is the "symplectic unit":

$$S = \begin{pmatrix} 0 & -1 \\ 1 & 0 \end{pmatrix}, \tag{43}$$

where 1 represents the identity matrix in $3N$-dimensions. Using a generalization of the algorithm for explicitly computing derivatives of computational algorithms, we can compute the Jacobian matrix for the evolution mapping defined by any integration scheme.

We denote by dI the relative change in the sum of the absolute values of the diagonal from lower left to upper right between $J^T S J$ and S. If equation (42) holds, $dI = 0$. We compare dI from the individual and adaptive timestep integrator described in this paper to dI from a standard individual and adaptive timestep Hermite integrator (Makino 1991). It is difficult to precisely control the stepsizes chosen in an adaptive timestep scheme, so we measure dI as a function of the total number of steps taken for the evolution, $n_{\rm steps}$. An error which scales as h^r should scale as $n_{\rm steps}^{-r}$.

Based on the discussion in Section 2.1.2, we expect that dI from the variational integrator will be fifth order (that is, it scales as n_{steps}^{-5}), while dI from the Hermite integrator will be fourth order (exactly the same order as the integrator's trajectory error). Figures 5 and 6 demonstrate that this is exactly the case for simulations of a Plummer initial condition with $N = 25$ bodies and varying numbers of steps. Scaling these results to an accuracy of $dI = 10^{-10}$ implies that the Hermite algorithm would require 1.5×10^6 steps to achieve this accuracy, while our algorithm would require 0.63×10^6 steps. Since there are two potential evaluations per step in our algorithm and one for the Hermite scheme, that translates to a 20% advantage in potential evaluations for our algorithm at an accuracy of $dI = 10^{-10}$.

Because they both depend on the accuracy of the solution to the implicit equation (16a), we expect that symplecticity and angular momentum conservation error would scale similarly in a long-term simulation. Results in the next section show that angular momentum error in a long-running simulation is two orders of magnitude less than the energy conservation error (Figure 7) using our algorithm, while the Hermite algorithm produces angular momentum errors commensurate with its energy conservation error.

6.2.2. 1000-body Cluster Simulation

Here we compare a 1000-body cluster simulation run using our variational integrator with another such simulation using the NBODY2h code (Aarseth 2001). NBODY2h is not the state-of-the-art in cluster simulations; it is an appropriate comparison to our code because it uses the state-of-the-art Hermite integration algorithm but uses softening instead of treating close encounters specially. We have run many such simulations—the one described here is typical. Recall we use the standard units: the total system mass is $M = 1$, $G = 1$, and the total energy $E = -1/4$ (Heggie & Mathieu 1986). In standard units, the virial radius of the system is 1. Initial conditions for both runs are a randomly sampled Plummer model shifted into a coordinate system where the center of mass is at the origin and the total linear momentum is zero.

In the simulation reported here, we chose to keep energy conservation to better than a part in 5×10^{-9} per unit timestep, with a target of one part in 10^{-9}. If, at the end of an advancement by $\Delta t = 1.0$, the relative energy error was greater than 5×10^{-9} we re-started the step with a smaller η parameter (cf. eq. (37)); at the end of every unit time interval, we adjusted η according to

$$\eta' = \eta \frac{10^{-9}}{\Delta E/E}. \tag{44}$$

Figure 7 shows the time-evolution of the relative energy error and relative angular mo-

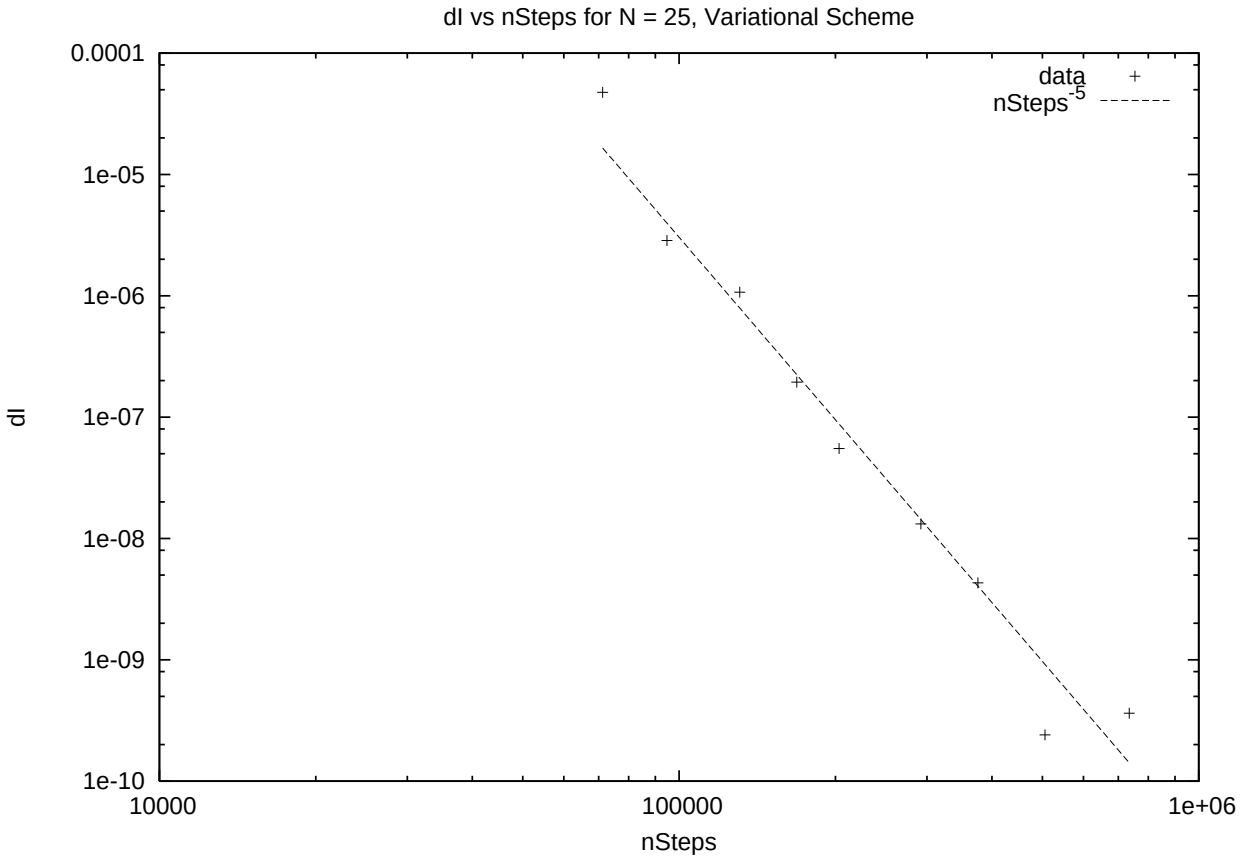

Fig. 5.— Scaling of the error in equation (42) (non-conservation of the Poincaré integral invariant) in multiple integrations of the same $N = 25$ Plummer initial condition over a unit time interval with varying numbers of steps using the variational integrator. The fitted line is $dI \propto n_{\rm steps}^{-5}$; the behavior is exactly as discussed in Section 2.1.2.

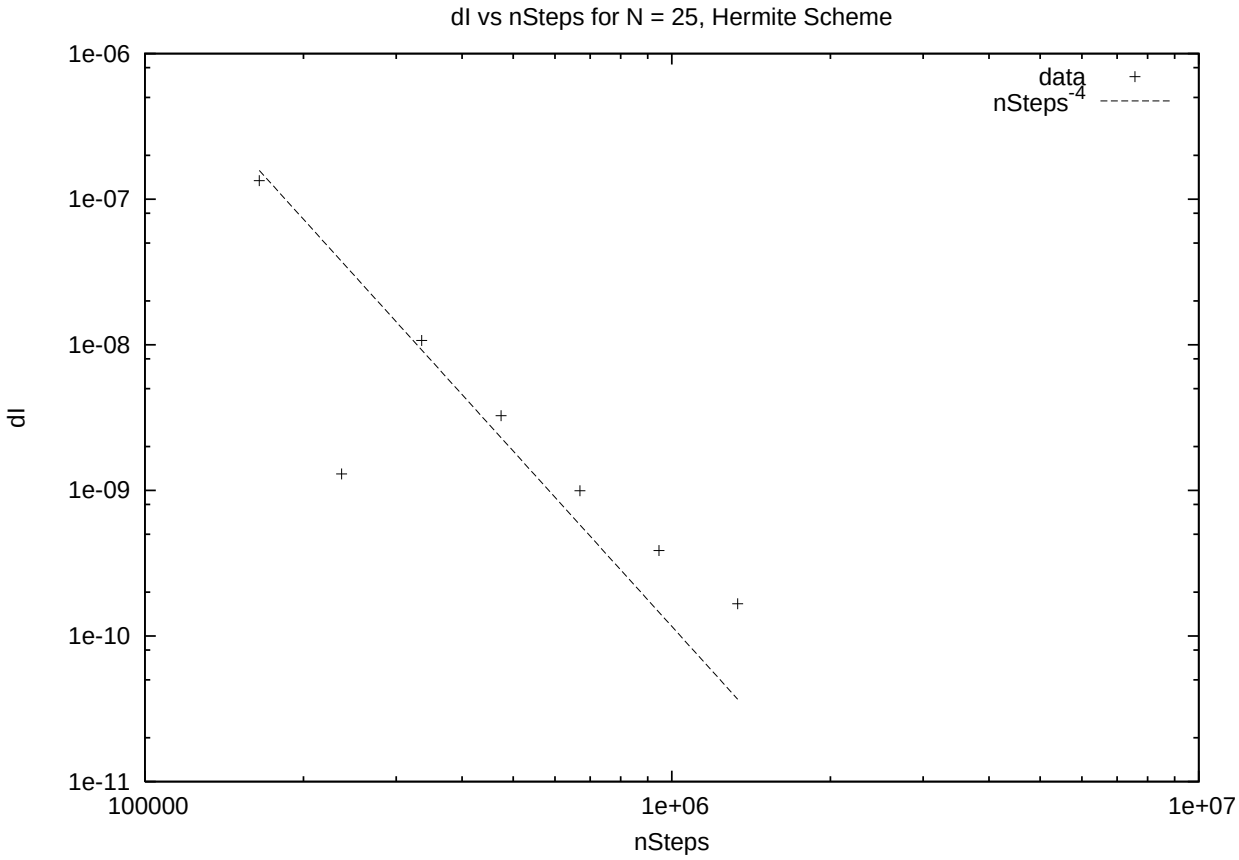

Fig. 6.— Scaling of the error in equation (42) (non-conservation of the Poincaré integral invariant) in multiple integrations of the same $N = 25$ Plummer initial condition over a unit time interval with varying numbers of steps using the Hermite integrator. The fitted line is $dI \propto n_{\rm steps}^{-4}$; the behavior is what would be expected from a fourth-order traditional integrator.

mentum error. Because of the reciprocity in potential evaluations, the integrator exactly conserves linear momentum (even if not iterating equation (16a) to convergence), but we expect, based on the discussion in Section 2.1.2, that the error in angular momentum conservation due to a single iteration of equation (16a) to scale as one power of h better than the energy (or trajectory) error. We can see in Figure 7 that the angular momentum conservation error is, in fact, about two orders of magnitude smaller than the energy conservation error.

Figure 8 compares the core radius (computed as described in Casertano & Hut (1985)) versus time for the variational simulation with the core radius output by the NBODY2 simulation. The radii are commensurate until about $r_c = 0.04$. We believe that the deviation after this point is due to random fluctuations, and is not physically significant. The NBODY2 simulation has momentum (both linear and angular) conservation error which is approximately commensurate with its energy conservation error—about two orders of magnitude worse than the variational algorithm's angular momentum conservation error, and six orders of magnitude worse than its linear momentum conservation error. Its wall-clock time is significantly better than the variational algorithm because our algorithm does not implement the nearest-neighbor scheme of Ahmad & Cohen (1973), and therefore evaluates all 999 potentials involving the body with the smallest timestep every step, all other 998 potentials involving the body with the second-smallest timestep every step for that body, etc.

7. Discussion

We have presented a class of N-body integrators obtained by discretizing the action as opposed to discretizing the equations of motion. Such integrators automatically conserve discrete momenta and are symplectic. This paper focuses on the fourth-order, three-point GGL integrator described in Section 2.1.2, but Section 2 describes a general framework for constructing such integrators. We have demonstrated, theoretically in Section 3 and experimentally in Section 6.1, that adaptive timestepping integrators can still be symplectic if they use a block-power-of-two scheme. Individual timesteps (Section 4) impose requirements that reduce the symplecticity and angular momentum conservation from exact to fifth-order (one order better than the trajectory error of our integrator); nevertheless, we have shown experimentally in Sections 6.2.1 and 6.2.2 that the benefits of fifth-order symplecticity and angular momentum conservation are significant.

Though our code is not CPU-time competitive with standard stellar-cluster simulations due to their use of the Ahmad-Cohen nearest-neighbor scheme, we expect it will be useful

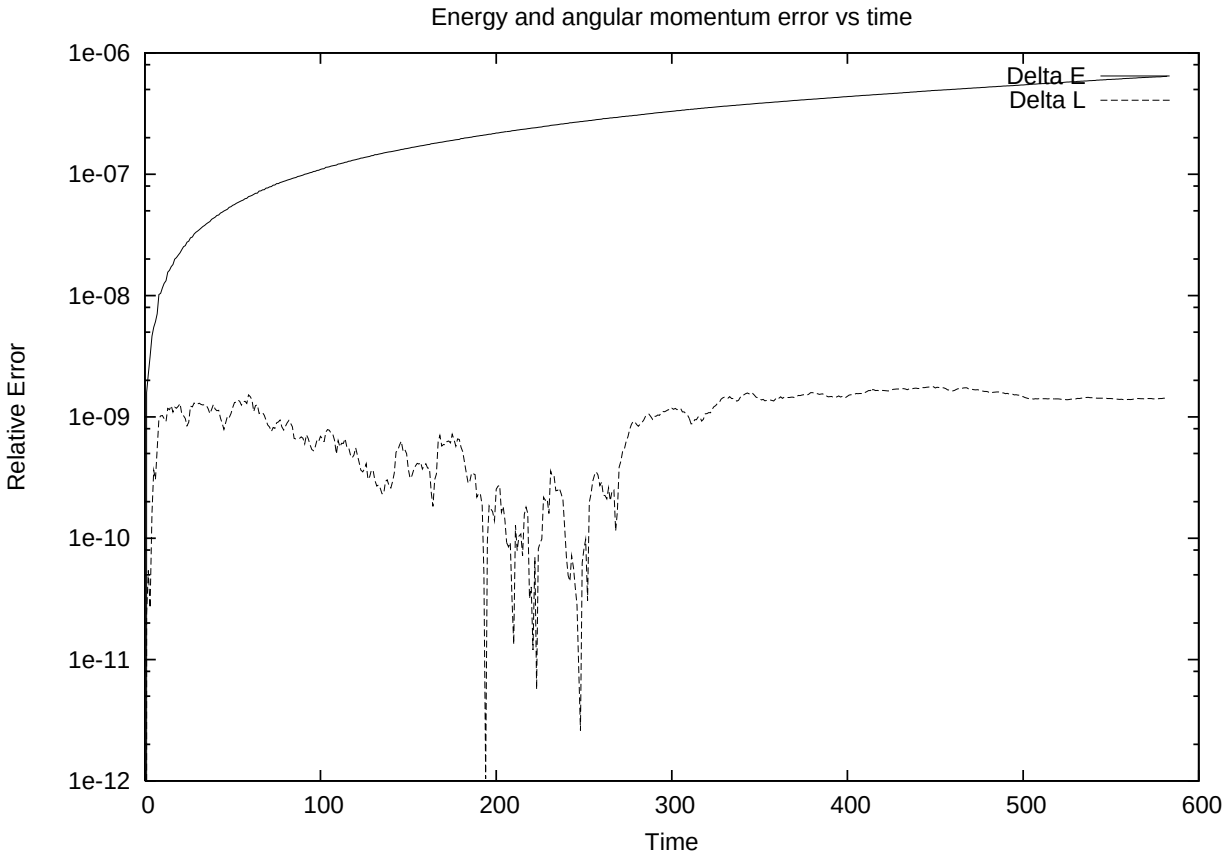

Fig. 7.— Relative energy and angular momentum conservation error for the 1000-body simulation performed using the variational integrator. As expected based on the discussion in Section 2.1.2, the angular momentum conservation error is much better than the energy conservation error.

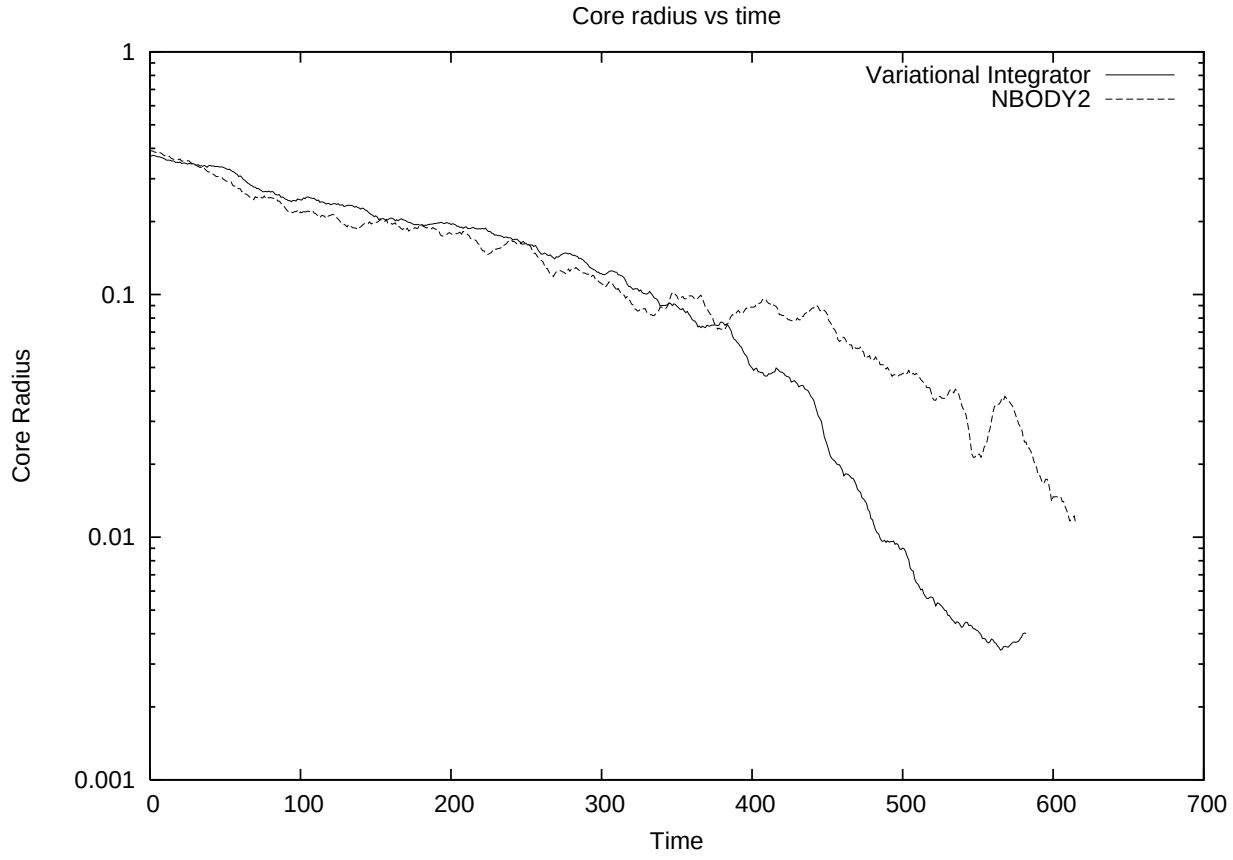

Fig. 8.— Core radius versus time for the simulation described in the text using the integrator in this paper and an equivalent simulation using the NBODY2 code. Boxcar averaging has been employed with $\Delta t = 15$ to reduce fluctuations in the curves.

in direct-summation N-body simulations where phase space volume conservation is more important than raw speed — though it would be interesting to see whether the Ahmad-Cohen scheme significantly affects the symplecticity of our algorithm in practice, we have not investigated this. We intend to use our algorithm to check the accuracy of dark matter halo evolution in larger, cosmological N-body simulations, and to investigate the formation of caustics in dark-matter distributions on a smaller scale. In these applications symplecticity is essential because the "coldness" of the dark matter phase-space distribution is fundamental to the dynamics.

Additionally, the algorithm was designed with the application to full cosmological N-body simulations in mind. The original motivation for the work was to find a higher-order, symplectic algorithm which takes only forward steps as an alternative to the leapfrog algorithm used in cosmological simulations. Standard higher-order symplectic integrators are not useful in this context because the simulations of gas dynamics in high-accuracy cosmological simulations become unstable under evolution backward in time, and these integrators all have backwards timesteps. We intend to explore this application in a future paper.

We would like to thank Jack Wisdom and Gerry Sussman for helpful discussions, encouragement, and inspiration. This work was supported by NSF grant AST-0407050 and NASA grant NNG06-GG99G.

REFERENCES

Aarseth, S. J. 2001, New Astronomy, 6, 277

Abramowitz, M. & Stegun, I. A., eds. 1972, Handbook of Mathematical Functions, With Formulas, Graphs and Mathemacial Tables (Dover Publications, Inc.)

Ahmad, A. & Cohen, L. 1973, Journal of Computational Physics, 12, 389

Casertano, S. & Hut, P. 1985, ApJ, 298, 80

Chambers, J. E. 2003, AJ, 126, 1119

Chin, S. A. & Chen, C. R. 2003, Unpublished: astro-ph/0304223

Ge, Z. & Marsden, J. E. 1988, Physics Letters A, 133, 134

Heggie, D. & Hut, P. 2003, The Gravitational Million-Body Problem (Cambridge University Press)

Heggie, D. & Mathieu, R. 1986, in The Use of Supercomputers in Stellar Dynamics, ed. S. McMillan & P. Hut (Springer), 233

Hut, P. & Makino, J. 2006, The Art of Computational Science: How to build a computational lab, Web: http://www.artcompsci.org/

Lew, A., Marsden, J. E., Ortiz, M., & West, M. 2004, Int. J. Numer. Meth. Engng, 60, 153

Makino, J. 1991, ApJ, 369, 200

Makino, J., Hut, P., Kaplan, M., & Saygin, H. 1996, NewA, 12, 123

Marsden, J. E. & West, M. 2001, Acta Numerica, 357

Preto, M. & Tremaine, S. 1999, AJ, 118, 2532

Scuro, S. R. & Chin, S. A. 2005, Physical Review E, 71, 056703

Sheng, Q. 1989, IMA Journal of Numerical Analysis, 9, 199

Shirokov, A. & Bertschinger, E. 2005, astro-ph/0505087

Springel, V. 2005a, private communication

—. 2005b, Monthly Notices of the Royal Astronomical Society, 364, 1105

Sussman, G. J. 2006, private communication

Sussman, G. J., Wisdom, J., & Mayer, M. E. 2001, Structure and Interpretation of Classical Mechanics (The MIT Press)

Suzuki, M. 1991, Journal of Mathematical Physics, 32, 400

Wisdom, J. & Holman, M. 1991, The Astronomical Journal, 102, 1528

Wisdom, J., Holman, M., & Touma, J. 1996, Fields Institute Communications, 10, 217

Yoshida, H. 1993, Celestial Mechanics and Dynamical Astronomy, 56, 27